Letter

Role of Debye temperature in achieving large adiabatic temperature changes at cryogenic temperatures: A case study on Pr_2In

Wei Liu,[1,*] Franziska Scheibel,[1] Nuno Fortunato,[1] Imants Dirba,[1] Tino Gottschall,[2] Hongbin Zhang,[1] Konstantin Skokov,[1] and Oliver Gutfleisch[1]

[1]*Institute of Materials Science, Technical University of Darmstadt, 64287 Darmstadt, Germany*

[2]*Dresden High Magnetic Field Laboratory (HLD-EMFL), Helmholtz-Zentrum Dresden-Rossendorf, 01328 Dresden, Germany*

(Received 9 November 2023; revised 4 March 2024; accepted 20 March 2024; published 17 April 2024)

The excellent magnetic entropy change (ΔS_T) in the temperature range of 20 ∼ 77 K due to the first-order phase transition makes Pr_2In an intriguing candidate for magnetocaloric hydrogen liquefaction. As an equally important magnetocaloric parameter, the adiabatic temperature change (ΔT_{ad}) of Pr_2In associated with the first-order phase transition has not yet been reported. In this work, the ΔT_{ad} of Pr_2In is obtained from heat capacity measurements: 2 K in fields of 2 T and 4.3 K in fields of 5 T. While demonstrating a ΔT_{ad} that is not as impressive as its remarkable ΔS_T, Pr_2In exhibits a low Debye temperature (T_D) of around 110 K. Based on these two observations, an approach that combines the mean-field and Debye models is developed to study the correlation between ΔT_{ad}, one of the most important magnetocaloric parameters, and T_D, one important property of a material. The role of T_D in achieving large ΔT_{ad} is revealed: materials with higher T_D tend to exhibit larger ΔT_{ad}, particularly in the cryogenic temperature range. This discovery explains the absence of an outstanding ΔT_{ad} in Pr_2In and can serve as a tool for designing or searching for materials with both a large ΔS_T and a ΔT_{ad}.

DOI: 10.1103/PhysRevB.109.L140407

Introduction. Magnetocaloric materials with large isothermal magnetic and adiabatic temperature changes (ΔS_T and ΔT_{ad}) in the temperature range from 20 K (condensation point of H_2) to 77 K (condensation point of N_2) are required for the successful implementation of magnetocaloric hydrogen liquefaction [1–5], an emerging cooling technology based on the magnetocaloric effect with great potential to achieve higher efficiency than the conventional liquefaction methods based on Joule-Thomson expansion [6–9]. In this sense, rare-earth-based intermetallic compounds are promising candidates for magnetocaloric hydrogen liquefaction [1,2,10–13]. In particular, the heavy rare-earth-based (Gd, Tb, Dy, Ho, Er, and Tm) ones such as HoB_2 [14], $ErAl_2$ [15], and $ErCo_2$ [16] have been intensively investigated due to their large magnetocaloric effects within the temperature range of 20 ∼ 77 K.

Although light rare-earth elements (La, Ce, Pr, Nd, and Sm) typically have a much lower resource criticality than heavy rare-earth elements, and therefore are more suitable for large-scale applications of magnetocaloric hydrogen liquefaction, light rare-earth-based intermetallic compounds are often overlooked because they generally show a weaker magnetocaloric effect than their heavy rare-earth counterparts [1]. The larger magnetocaloric effects of heavy rare-earth-based materials are attributed to the larger magnetic moments of heavy rare-earth ions [1]. The light rare-earth ions, namely Ce^{3+}, Pr^{3+}, Nd^{3+}, and Sm^{3+}, have a magnetic moment below 4 μ_B, much smaller than the heavy rare-earth ions of Gd^{3+}, Tb^{3+}, Dy^{3+}, Ho^{3+}, Er^{3+}, and Tm^{3+}, which show a magnetic moment greater than 7 μ_B [17].

However, the report on Pr_2In showing an excellent ΔS_T of about 20 J K^{-1} kg^{-1} in magnetic fields of 5 T at about 57 K [18] opens a new pathway that breaks the aforementioned stereotype. Although known for demonstrating the strongest magnetocaloric effect among the heavy rare-earth R_2In (R: Gd, Tb, Dy, Ho, and Er) system [19], the second-order magnetocaloric material Er_2In with a Curie temperature (T_C) of 20 K exhibits a ΔS_T of 15.5 J K^{-1} kg^{-1}, significantly smaller than Pr_2In. The giant ΔS_T within the temperature range of 20 ∼ 77 K makes Pr_2In an attractive candidate for magnetocaloric hydrogen liquefaction.

The giant ΔS_T in Pr_2In is ascribed to its first-order magnetic phase transition [18,20]. This alloy, as well as Nd_2In and Eu_2In, was initially reported to show a first-order phase transition by Forker *et al.* in 2005, evidenced by the measurements of magnetic and electric hyperfine interactions [21]. Subsequently, in 2018 Guillou *et al.* reported the giant first-order magnetocaloric effect in Eu_2In [22], triggering a series of experimental and theoretical studies on this compound and its relatives [23–26]. It is worth mentioning that Tapia-Mendive *et al.* theoretically demonstrated that the first-order phase transition in Eu_2In is due to a topological change to the Fermi surface [24].

Soon after the observation of the giant ΔS_T in Eu_2In, the excellent ΔS_T in Pr_2In [20] and Nd_2In [27,28] were reported. It is worth mentioning that there is also a study reporting that Pr_2In exhibits a second-order phase transition without a significantly large ΔS_T [29]. The reason for this discrepancy

*wei.liu@tu-darmstadt.de

is not yet clear and could be attributed to differences in sample preparation and heat treatment.

Despite the fact that ΔT_{ad} is as important as ΔS_T for the magnetocaloric effect [30], ΔT_{ad} of Pr_2In showing a first-order magnetic phase transition remains unreported. The first part of our work is about revisiting Pr_2In to obtain its ΔT_{ad} by constructing the total entropy curves from heat capacity data. The discoveries of the absence of an outstanding ΔT_{ad} and the low Debye temperature (T_D) in Pr_2In motivate us to study the correlation between ΔT_{ad} and T_D to explain why Pr_2In shows no remarkable ΔT_{ad} and explore ways to improve this important magnetocaloric parameter.

Experiment. Pr_2In was synthesized by arc-melting high-purity raw materials Pr (99.5 wt.% pure) and In (99.99 wt.% pure) five times. To ensure good homogeneity, the ingot was flipped after each melting. As the surface of the Pr_2In sample reacts with air, the ground powder was sealed in a capillary hermetically in an Ar-filled glovebox [$p(O_2) < 0.1$ ppm] for powder x-ray diffraction (XRD). The powder XRD measurement was performed using a powder diffractometer (Stadi P, Stoe & Cie GmbH) equipped with a Ge111-Monochromator using MoKα_1 radiation ($\lambda = 0.70930$ Å) in the DebyeScherrer geometry. Magnetization as a function of temperature in magnetic fields up to 10 T were measured by a Physical Property Measurement System (PPMS) from Quantum Design. Heat capacity in magnetic fields of 0, 1, 2, 5, and 10 T was measured in the same PPMS with the 2τ approach.

Results and discussion, Phase purity. The sufficient purity of the Pr_2In crystallizing in Ni_2In-type hexagonal structure (space group: $P6_3/mmc$) is confirmed by the XRD measurement. The XRD patterns and the results of Rietveld refinement are included in the Supplemental Material [31].

Magnetocaloric properties. This part focuses on the magnetocaloric properties of Pr_2In. Figure 1(a) displays the magnetization (M) vs temperature (T) curves of Pr_2In in magnetic fields of 0.02, 1, 2, 5, and 10 T. Two transitions are observed: one at 56 K and the other at about 35 K. The transition at about 35 K was reported to be a possible spin reorientation transition [20]. The transition at 56 K was reported to be a first-order magnetic phase transition with an excellent ΔS_T of 15 J K^{-1} kg^{-1} in magnetic fields of 2 T [20].

Figure 1(b) presents the ΔS_T of Pr_2In as a function of temperature in magnetic fields of 0.5, 1, 1.5, and 2 T. ΔS_T is calculated from MT measurements [shown in the inset in Fig. 1(a)] with a magnetic field step of 0.25 T. This calculation is based on the Maxwell relation via the equation $\Delta S_T = \int_0^H \mu_0(\partial M/\partial T)_H\, dH$ [32]. The ΔS_T calculated from MT measurements reaches 17.5 J K^{-1} kg^{-1} in magnetic fields of 2 T at 56.5 K, which is slightly higher than the value reported in Ref. [20]. To confirm that the nature of the phase transition at about 56 K is first order, we calculated the exponent n from the power law $\Delta S_T \propto H^n$ [33] and plotted it as a function of temperature in the inset in Fig. 1(b). The n values in all fields overshoot two, confirming the nature of the first-order phase transition.

ΔS_T can also be obtained from the S(T,H) curves constructed from the heat capacity data by equation $S(T,H) = \int_0^T \mu_0(C_p(T,H)/T)\, dT$ [32]. After constructing the *S(T,H)* curves, ΔS_T is calculated by [34]

$$\Delta S_T(T,H) = S(T,H) - S(T,0). \tag{1}$$

The detailed procedure for calculating ΔS_T from heat capacity data is included in the Supplemental Material [31]. Figure 1(c) plots the ΔS_T obtained from heat capacity data in magnetic fields of 1, 2, 5, and 10 T, and ΔS_T from MT measurements in magnetic fields of 1 and 2 T. The ΔS_T from heat capacity measurements matches well with the ΔS_T from magnetization measurements, confirming the accuracy of the heat capacity measurements. In magnetic fields of 10 T, ΔS_T reaches a value of about 25 J K^{-1} kg^{-1}, and a plateaulike step emerges on the peak of the $\Delta S_T(T)$ curves, which is a character of first-order phase transitions [35].

Figure 1(d) shows the ΔT_{ad} indirectly obtained from heat capacity measurements in magnetic fields of 1, 2, 5, and 10 T. ΔT_{ad} is obtained from the constructed $S(T,H)$ curves via [34]

$$\Delta T_{ad}(T = T(S,0), H) = T(S,H) - T(S,0), \tag{2}$$

where $T(S,H)$ is the inverse function of $S(T,H)$. The detailed process for calculating ΔT_{ad} from the heat capacity data is included in the Supplemental Material [31]. In magnetic fields of 2 and 5 T, the ΔT_{ad} of Pr_2In reach 2 and 4.3 K, respectively.

However, these two values are not as impressive as the remarkable ΔS_T in Pr_2In. Figures 1(e) and 1(f) compare ΔS_T and ΔT_{ad} of Pr_2In with other light and heavy rare-earth-based magnetocaloric materials in magnetic fields of 5 T. The ΔS_T of Pr_2In is not only significantly larger than that of Er_2In, but also larger than $Pr_{0.75}Ce_{0.25}Al_2$, which shows the largest ΔS_T among the light rare-earth-based Laves phase RAl_2 series, and the heavy rare-earth-based Laves phase $DyAl_2$, known as a promising candidate for magnetocaloric hydrogen liquefaction [39]. However, Pr_2In has a much smaller ΔT_{ad} than $DyAl_2$ despite that Pr_2In shows a larger ΔS_T. The ΔT_{ad} of $DyAl_2$ is about 1.5 times as large as that of Pr_2In.

Since ΔT_{ad} is indirectly obtained from the heat capacity measurement, a close look is given to the heat capacity data. Figure 2(a) shows the total isobaric heat capacity C_{tot} of Pr_2In in magnetic fields of 0, 1, 2, 5, and 10 T. One observation is that the peak of the heat capacity curves shifts with H, implying a first-order phase transition [36]. Another observation is that C_{tot} of Pr_2In is almost constant even near 80 K, indicating a low Debye temperature T_D. Due to the two magnetic phase transitions at low temperature, it is difficult to obtain T_D from the linear relation $C_{tot}/T \propto \alpha T^2 + \gamma$ (α is the slope in which T_D can be calculated, and γ is the Sommerfeld coefficient) [40]. In the literature, it is common to use the Debye model to fit heat capacity data to obtain T_D [41–43]. This approach is based on the following equation:

$$C_V + C_e = 9Nk_B\left(\frac{T}{T_D}\right)^3 \int_0^{T_D/T} \frac{x^4 e^x}{(e^x-1)^2} dx + \gamma T, \tag{3}$$

where N is the number of atoms, C_V is the volumetric lattice heat capacity, C_e is the electronic heat capacity, k_B is the Boltzmann constant, and $x = h\nu/k_B T$ with ν to be the frequency of the phonon.

In the present work, we obtained a Debye temperature of around 110 K for Pr_2In using Eq. (3). This value is small, being outside the range of 200 ∼ 400 K where T_D of most

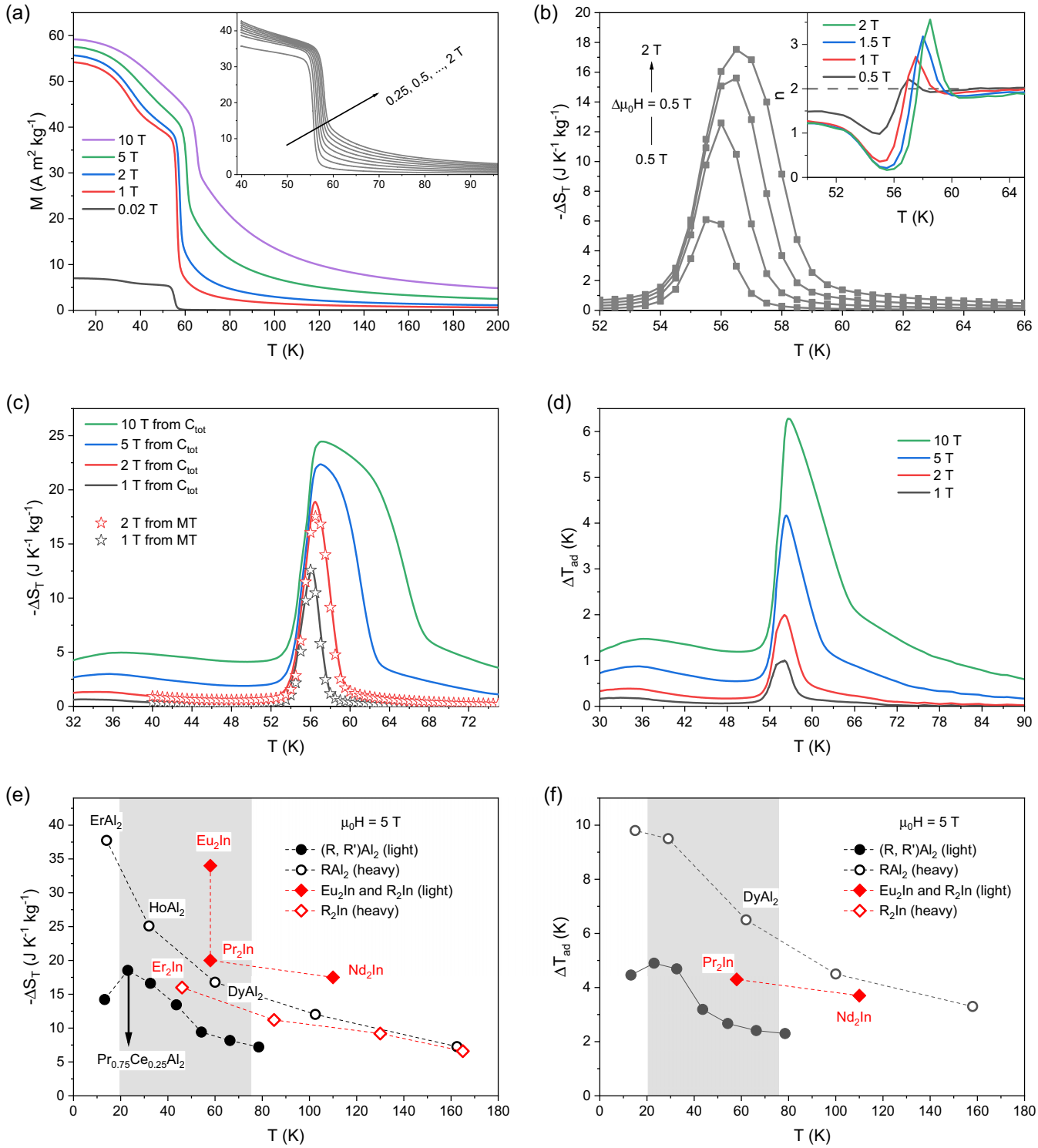

FIG. 1. (a) Magnetization of Pr_2In as a function of temperature. (b) ΔS_T of Pr_2In from magnetization measurements. The inset shows the exponent n ($|\Delta S_T| \propto H^n$) vs T. (c) ΔS_T of Pr_2In from MT measurements and heat capacity measurements. (d) ΔT_{ad} from heat capacity measurements. (e), (f) ΔS_T and ΔT_{ad} for light and heavy rare-earth-based R_2In [18,19,22,28,36–38], RAl_2 (Pr, Nd, Gd, Tb, Dy, Ho, Er) [1,2,16] in magnetic fields of 5 T. The shadows mark the range of 77 ∼ 20 K.

alloys lie [40]. A similar small value of about 120 K was also reported for Yb_2In, an intermetallic compound that adopts the same crystal structure as Pr_2In [25]. Figure 2(b) plots the the volumetric lattice heat capacity C_V for different Debye temperatures from 110 to 410 K with a step of 50 K using the Debye model. A significant difference between C_V at cryogenic temperatures and near room temperature is revealed: C_V for $T_D \leqslant 410$ K at 300 K are close, but at cryogenic

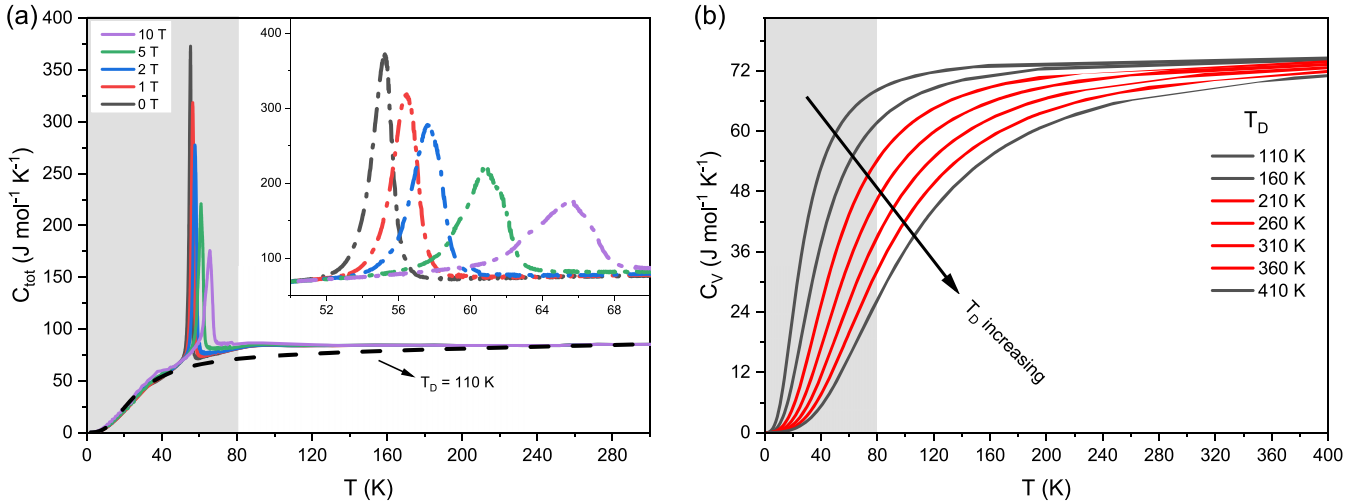

FIG. 2. (a) Heat capacity of Pr_2In as a function of temperature in magnetic fields of 0, 1, 2, 5, and 10 T. (b) Volumetric lattice heat capacity from Debye model with T_D varying from 110 to 410 K with a step of 50 K.

temperatures such as 60 K, C_V for $T_D < 210$ K shows a significantly higher value. The difference between C_V at cryogenic temperatures and near room temperature for different T_D has led us to think about how ΔT_{ad} correlates with T_D.

Neglecting the electronic entropy as it is usually small compared to the magnetic entropy S_m and the lattice entropy S_l [45], the total entropy can be calculated by

$$S(T,H) = S_m + S_l. \tag{4}$$

The magnetic entropy is given by [32,44]

$$S_m = N_M k_B \left[\ln \frac{\sinh\left(\frac{2J+1}{2J}y\right)}{\sinh\left(\frac{1}{2J}y\right)} - yB_J(y) \right], \tag{5}$$

with N_M the number of magnetic atoms, J the total angular momentum, $B_J(x)$ the Brillouin function, and

$$y = \frac{g_J J \mu_B \mu_0 H + \frac{3J}{J+1} k_B T_C B_J(y)}{k_B T}, \tag{6}$$

where g_J is the Landé g factor, T_C the Curie temperature, and μ_0 the vacuum permeability.

The equation to calculate the lattice entropy S_l is given by [45]

$$S_l = -3Nk_B \left[\ln\left(1 - \exp\left(-\frac{T_D}{T}\right)\right)\right] + 12Nk_B \left(\frac{T}{T_D}\right)^3 \int_0^{T_D/T} \frac{x^3}{\exp(x) - 1} dx. \tag{7}$$

Equations (2), (4), (5), and (7) connect ΔT_{ad} with T_D. By varying T_D and T_C, we can see how ΔT_{ad} changes. However, it should be emphasized that these equations only take J, g_J, T, T_C, and T_D as variables. In the present work, we only consider these parameters, ignoring the rest of the factors such as microstructures and stoichiometry that influence ΔT_{ad}. In the present work, the values of J and g_J are taken as 4 and 4/5, respectively, which corresponds to Pr^{3+}.

The calculated ΔS_T and ΔT_{ad} using Eqs. (2), (4), (5), and (7) with T_D and T_C varying are displayed in Figs. 3(a) and 3(b). Equation (5) implies that ΔS_T does not depend on T_D; ΔS_T should have the same value at the same T_C regardless of how T_D is varying. This is the reason why there is only one $\Delta S(T_C, T_D)$ curve in Fig. 3(a). However, this is not the case for ΔT_{ad}. In Fig. 3(b), different T_D leads to a different $\Delta T_{ad}(T_C)$ curve. It can be observed that T_D influences the turning point where the decreasing trend of the maximum ΔT_{ad} with respect to the decreasing T_C turns to an increasing trend: for T_D= 110 K, the increasing trend is not observed until 30 K, while for T_D= 410 K, an increasing trend starts at 120 K. It can be concluded that material systems with higher T_D tend to exhibit larger ΔT_{ad}, particularly in the cryogenic temperature range. From the inset in Fig. 3(b), the ΔT_{ad} of the material with a T_D= 360 K is more than twice as large as the material with a T_D = 110 K, although both have the same maximum ΔS_T at 56.5 K.

It should be noted that there are no ideal material systems that only vary in T_C and T_D while keeping the remaining parameters constant. Furthermore, although the correlation between ΔT_{ad} and T_D can be well described by the approach that combines the mean-field theory and the Debye model, further improvements are needed to include the factor of the nature of the phase transition order for a more profound interpretation. In particular, the nature and mechanism of the first-order phase transition of Pr_2In are not yet fully understood. Further theoretical and experimental investigations are required, such as the topological change of the Fermi surface of Pr_2In and its magnetic configurations. Moreover, ΔS_T and ΔT_{ad} are influenced by many factors, including extrinsic factors such as grain size and texture, and intrinsic factors such as crystalline electric field and stoichiometry [2,46–48]. It should be also emphasized that the shifting of the transition temperature with respect to magnetic fields also influences ΔT_{ad} for first-order phase transitions [49–51]. The relatively small dT_C/dH (about 1 K/T for Pr_2In) also contributes to the absence of an excellent ΔT_{ad} in Pr_2In. Nevertheless, the mean-field approach presented in this work provides a way of understanding the absence of an outstanding ΔT_{ad} in Pr_2In.

For a more generic interpretation on how T_D influences ΔT_{ad}, we consider the total entropy curve. Figure 3(c) shows

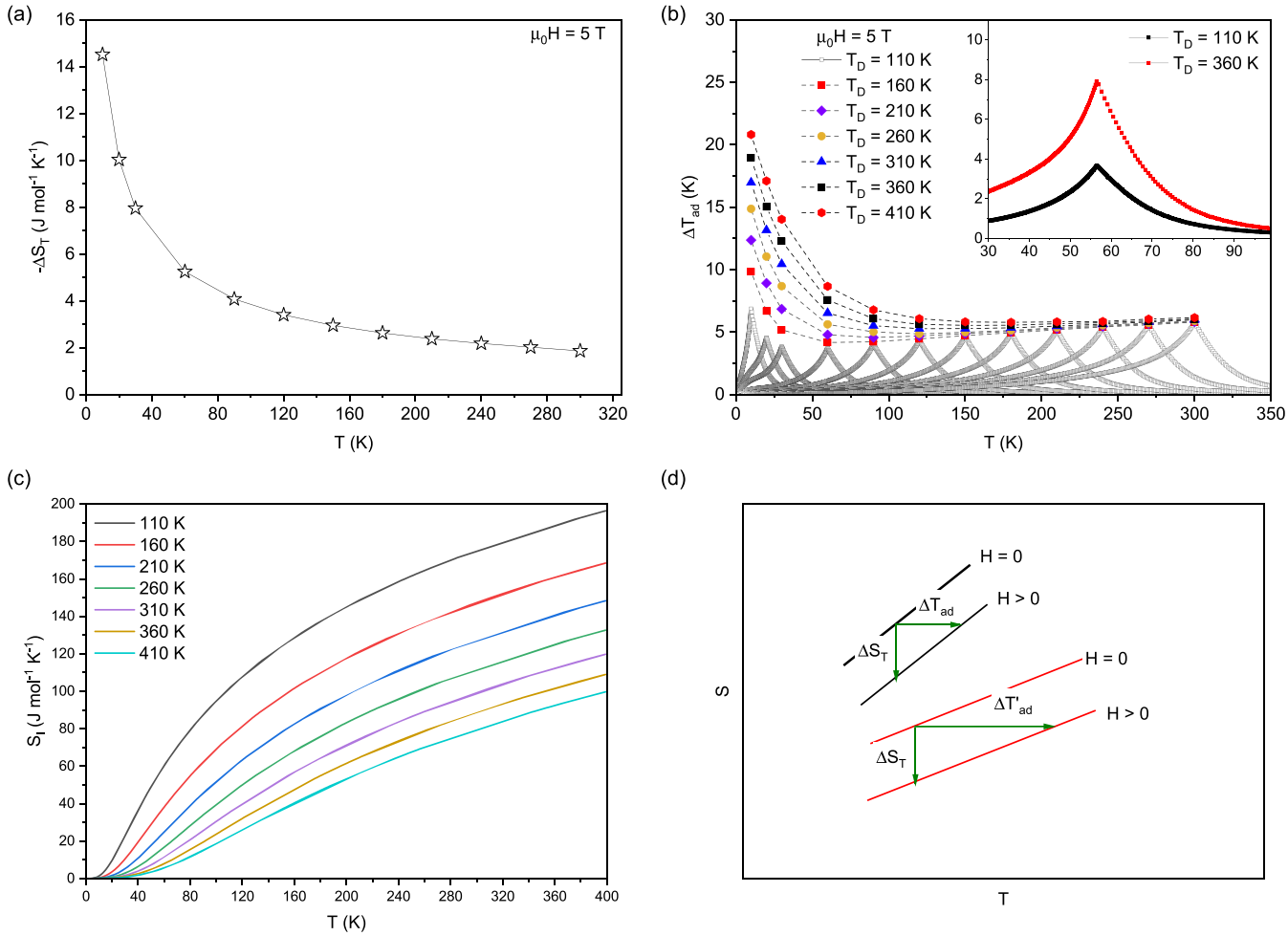

FIG. 3. (a) ΔS_T calculated from the mean-field approach. (b) ΔT_{ad} calculated from the mean-field theory with T_C and T_D varying. The inset compares the ΔT_{ad} for $T_D = 110$K and 360 K with both $T_C = 56.5$K. (c) Lattice entropies for different T_D. (d) Illustration of how the slope of the entropy curve influences ΔT_{ad}.

the lattice entropy S_l for different T_D. As observed, in cryogenic temperature range, the S_l curve for smaller T_D tends to exhibit a larger slope. Supposing that S_m are all the same for all the T_D, it can be concluded that in the cryogenic temperature range, the slope of the total entropy $S(T, H)$ is larger for smaller T_D since

$$\frac{dS(T,H)}{dT} = \frac{dS_l(T)}{dT} + \frac{dS_m(T,H)}{dT}. \tag{8}$$

As illustrated in Fig. 3(d), a steeper $S(H, T)$ results in a smaller ΔT_{ad}, although both of them have the same ΔS_T. In addition, based on the fact that it is a characteristic of first-order phase transition that the peak of the heat capacity shifts with magnetic fields, another explanation of how T_D influences ΔT_{ad} for first-order phase transition is included in the Supplemental Material [31].

Conclusions. In this study, the ΔT_{ad} of Pr_2In showing a first-order magnetic phase transition with an excellent ΔS_T is obtained indirectly from heat capacity data: 2 and 4.3 K in magnetic fields of 2 and 5 T, respectively. Motivated by the observation that the ΔT_{ad} of Pr_2In is not as significant as its ΔS_T, research on Pr_2In continues to explain why an outstanding ΔT_{ad} in Pr_2In is absent. Inspired by the finding that Pr_2In shows a low T_D of around 110 K, the correlation between ΔT_{ad} and T_D is studied. Combining the mean-field model with the Debye model, it is shown that T_D has a substantial impact on ΔT_{ad}: materials with a higher T_D tend to show a larger ΔT_{ad}, particularly at cryogenic temperatures.

Our work makes a connection between T_D, an important physical quantity that correlates the elastic properties with the thermodynamic properties (such as phonons, thermal expansion, thermal conductivity, specific heat, and lattice enthalpy), and ΔT_{ad}, one of the most important magnetocaloric parameters [52]. The important role of T_D in achieving large ΔT_{ad} at cryogenic temperatures is demonstrated, which could guide the search or design of materials with both large ΔS_T and ΔT_{ad} by considering materials with high T_D. Furthermore, more research is required on the mechanism of the magnetocaloric effect in Pr_2In, since it is not yet fully understood. We should also explore ways to replace Indium as it is also a highly critical element.

The data that support the findings of this study are available upon reasonable request from the authors.

Acknowledgments. We gratefully acknowledge the support from HLD (Dresden High Magnetic Field Laboratory), from Deutsche Forschungsgemeinschaft (DFG, German Research Foundation) through the CRC/TRR 270 (Project ID 405553726 and ID 456263705), from European Research Council (ERC) under the European Unions Horizon 2020 research and innovation program (Grant No. 743116, Cool Innov), and from the Clean Hydrogen Partnership and its members within the framework of the project HyLICAL (Grant No. 101101461). We greatly appreciate the constructive discussions and useful experimental help from Marc Strassheim and Eduard Bykov from HLD, and Alex Aubert from TU Darmstadt.

[1] W. Liu, T. Gottschall, F. Scheibel, E. Bykov, N. Fortunato, A. Aubert, H. Zhang, K. P. Skokov, and O. Gutfleisch, Designing magnetocaloric materials for hydrogen liquefaction with light rare-earth laves phases, J. Phys. Energy **5**, 034001 (2023).

[2] W. Liu, E. Bykov, S. Taskaev, M. Bogush, V. Khovaylo, N. Fortunato, A. Aubert, H. Zhang, T. Gottschall, J. Wosnitza, F. Scheibel, K. Skokov, and O. Gutfleisch, A study on rare-earth laves phases for magnetocaloric liquefaction of hydrogen, Appl. Mater. Today **29**, 101624 (2022).

[3] X. Tang, H. Sepehri-Amin, N. Terada, A. Martin-Cid, I. Kurniawan, S. Kobayashi, Y. Kotani, H. Takeya, J. Lai, Y. Matsushita, T. Ohkubo, Y. Miura, T. Nakamura, and K. Hono, Magnetic refrigeration material operating at a full temperature range required for hydrogen liquefaction, Nat. Commun. **13**, 1817 (2022).

[4] H. Zhang, R. Gimaev, B. Kovalev, K. Kamilov, V. Zverev, and A. Tishin, Review on the materials and devices for magnetic refrigeration in the temperature range of nitrogen and hydrogen liquefaction, Chin. Phys. B **558**, 65 (2019).

[5] Y. S. Koshkid'ko, E. T. Dilmieva, A. P. Kamantsev, A. V. Mashirov, J. Cwik, N. B. Kol'chugina, V. V. Koledov, and V. G. Shavrov, Magnetocaloric materials for low-temperature magnetic cooling, J. Commun. Technol. Electron. **68**, 379 (2023).

[6] A. Kitanovski, Energy applications of magnetocaloric materials, Adv. Energy Mater. **10**, 1903741 (2020).

[7] K. Matsumoto, T. Kondo, M. Ikeda, and T. Numazawa, Numerical analysis of active magnetic regenerators for hydrogen magnetic refrigeration between 20 and 77k, Cryogenics **51**, 353 (2011).

[8] T. Feng, R. Chen, and R. V. Ihnfeldt, Modeling of hydrogen liquefaction using magnetocaloric cycles with permanent magnets, Int. J. Refrig. **119**, 238 (2020).

[9] J. Barclay, K. Brooks, J. Cui, J. Holladay, K. Meinhardt, E. Polikarpov, and E. Thomsen, Propane liquefaction with an active magnetic regenerative liquefier, Cryogenics **100**, 69 (2019).

[10] V. Franco, J. S. Blázquez, J. J. Ipus, J. Y. Law, L. M. Moreno-Ramírez, and A. Conde, Magnetocaloric effect: From materials research to refrigeration devices, Prog. Mater. Sci. **93**, 112 (2018).

[11] X.-Q. Zheng and B.-g. Shen, The magnetic properties and magnetocaloric effects in binary R – T (R = Pr, Gd, Tb, Dy, Ho, Er, Tm; T = Ga, Ni, Co, Cu) intermetallic compounds, Chin. Phys. B **26**, 027501 (2017).

[12] J. Y. Law, L. M. Moreno-Ramírez, Á. Díaz-García, and V. Franco, Current perspective in magnetocaloric materials research, J. Appl. Phys. **133**, 040903 (2023).

[13] L. Li and M. Yan, Recent progresses in exploring the rare earth based intermetallic compounds for cryogenic magnetic refrigeration, J. Alloys Compd. **823**, 153810 (2020).

[14] P. B. de Castro, K. Terashima, T. D. Yamamoto, Z. Hou, S. Iwasaki, R. Matsumoto, S. Adachi, Y. Saito, P. Song, H. Takeya, and Y. Takano, Machine-learning-guided discovery of the gigantic magnetocaloric effect in HoB_2 near the hydrogen liquefaction temperature, NPG Asia Mater. **12**, 35 (2020).

[15] S. Yang, X. Zheng, D. Wang, J. Xu, W. Yin, L. Xi, C. Liu, J. Liu, J. Xu, H. Zhang, Z. Xu, L. Wang, Y. Yao, M. Zhang, Y. Zhang, J. Shen, S. Wang, and B. Shen, Giant low-field magnetocaloric effect in ferromagnetically ordered $Er_{1-x}Tm_xAl_2$ ($0 \leqslant x \leqslant 1$) compounds, J. Mater. Sci. Technol. **146**, 168 (2023).

[16] L. A. Gil, J. Campoy, E. Plaza, and M. V. de Souza, Conventional and anisotropic magnetic entropy change in $HoAl_2$ ferromagnetic compound, J. Magn. Magn. Mater. **409**, 45 (2016).

[17] J. M. D. Coey, *Magnetism and magnetic materials* (Cambridge University Press, New York, 2009).

[18] A. Biswas, R. K. Chouhan, O. Dolotko, A. Thayer, S. Lapidus, Y. Mudryk, and V. K. Pecharsky, Correlating crystallography, magnetism, and electronic structure across anhysteretic first-order phase transition in Pr_2In, ECS J. Solid. State Sci. Technol. **11**, 043005 (2022).

[19] H. Zhang, B. G. Shen, Z. Y. Xu, J. Chen, J. Shen, F. X. Hu, and J. R. Sun, Large reversible magnetocaloric effect in Er_2In compound, J. Alloys Compd. **509**, 2602 (2011).

[20] A. Biswas, N. A. Zarkevich, A. K. Pathak, O. Dolotko, I. Z. Hlova, A. V. Smirnov, Y. Mudryk, D. D. Johnson, and V. K. Pecharsky, First-order magnetic phase transition in Pr_2In with negligible thermomagnetic hysteresis, Phys. Rev. B **101**, 224402 (2020).

[21] M. Forker, R. Müßeler, S. C. Bedi, M. Olzon-Dionysio, and S. D. de Souza, Magnetic and electric hyperfine interactions in the rare-earth indium compounds R_2In studied by ^{111}Cd perturbed angular correlations, Phys. Rev. B **71**, 094404 (2005).

[22] F. Guillou, A. K. Pathak, D. Paudyal, Y. Mudryk, F. Wilhelm, A. Rogalev, and V. K. Pecharsky, Non-hysteretic first-order phase transition with large latent heat and giant low-field magnetocaloric effect, Nat. Commun. **9**, 2925 (2018).

[23] D. H. Ryan, D. Paudyal, F. Guillou, Y. Mudryk, A. K. Pathak, and V. K. Pecharsky, The first-order magnetoelastic transition in Eu_2In: A ^{151}Eu Mössbauer study, AIP Adv. **9**, 125137 (2019).

[24] E. Mendive-Tapia, D. Paudyal, L. Petit, and J. B. Staunton, First-order ferromagnetic transitions of lanthanide local moments in divalent compounds: An itinerant electron positive feedback mechanism and fermi surface topological change, Phys. Rev. B **101**, 174437 (2020).

[25] F. Guillou, H. Yibole, R. Hamane, V. Hardy, Y. B. Sun, J. J. Zhao, Y. Mudryk, and V. K. Pecharsky, Crystal structure and physical properties of Yb_2In and $Eu_{2-x}Yb_xIn$ alloys, Phys. Rev. Mater. **4**, 104402 (2020).

[26] B. P. Alho, P. O. Ribeiro, P. J. von Ranke, F. Guillou, Y. Mudryk, and V. K. Pecharsky, Free-energy analysis of the nonhysteretic first-order phase transition of Eu_2In, Phys. Rev. B **102**, 134425 (2020).

[27] W. Liu, F. Scheibel, T. Gottschall, E. Bykov, I. Dirba, K. Skokov, and O. Gutfleisch, Large magnetic entropy change in Nd_2In near the boiling temperature of natural gas, Appl. Phys. Lett. **119**, 022408 (2021).

[28] A. Biswas, R. K. Chouhan, A. Thayer, Y. Mudryk, I. Z. Hlova, O. Dolotko, and V. K. Pecharsky, Unusual first-order magnetic phase transition and large magnetocaloric effect in Nd_2In, Phys. Rev. Mater. **6**, 114406 (2022).

[29] W. Cui, G. Yao, S. Sun, Q. Wang, J. Zhu, and S. Yang, Unconventional metamagnetic phase transition in R_2In (R=Nd, Pr) with lambda-like specific heat and nonhysteresis, J. Mater. Sci. Technol. **101**, 80 (2022).

[30] T. Gottschall, K. P. Skokov, M. Fries, A. Taubel, I. Radulov, F. Scheibel, D. Benke, S. Riegg, and O. Gutfleisch, Making a cool choice: The materials library of magnetic refrigeration, Adv. Energy Mater. **9**, 1901322 (2019).

[31] See Supplemental Material at http://link.aps.org/supplemental/10.1103/PhysRevB.109.L140407 for the xrd pattern and the results of rietveld measurement; the construction of the total entropy curves; and a way of understanding how t_d influences δt_{ad} in the case of first-order phase transition. The Supplemental Material also contains Refs. [20,35].

[32] A. M. Tishin and Y. I. Spichkin, *The Magnetocaloric Effect and its Applications*, Series in Condensed Matter Physics (Institute of Physics Pub, Bristol, UK, 2003).

[33] J. Y. Law, V. Franco, L. M. Moreno-Ramírez, A. Conde, D. Y. Karpenkov, I. Radulov, K. P. Skokov, and O. Gutfleisch, A quantitative criterion for determining the order of magnetic phase transitions using the magnetocaloric effect, Nat. Commun. **9**, 2680 (2018).

[34] V. K. Pecharsky and K. A. Gschneidner, Magnetocaloric effect from indirect measurements: Magnetization and heat capacity, J. Appl. Phys. **86**, 565 (1999).

[35] A. Smith, C. R. Bahl, R. Bjørk, K. Engelbrecht, K. K. Nielsen, and N. Pryds, Materials challenges for high performance magnetocaloric refrigeration devices, Adv. Energy Mater. **2**, 1288 (2012).

[36] Q. Zhang, J. H. Cho, J. Du, F. Yang, X. G. Liu, W. J. Feng, Y. J. Zhang, J. Li, and Z. D. Zhang, Large reversible magnetocaloric effect in Tb_2In, Solid State Commun. **149**, 396 (2009).

[37] Q. Zhang, J. H. Cho, B. Li, W. J. Hu, and Z. D. Zhang, Magnetocaloric effect in Ho_2In over a wide temperature range, Appl. Phys. Lett. **94**, 182501 (2009).

[38] Q. Zhang, X. G. Liu, F. Yang, W. J. Feng, X. G. Zhao, D. J. Kang, and Z. D. Zhang, Large reversible magnetocaloric effect in Dy_2In, J. Phys. D: Appl. Phys. **42**, 055011 (2009).

[39] P. O. Ribeiro, B. P. Alho, R. S. de Oliveira, E. P. Nóbrega, V. de Sousa, P. J. von Ranke, Y. Mudryk, and V. K. Pecharsky, Magnetothermal properties of $Tm_xDy_{1-x}Al_2$ (x= 0.25, 0.50 and 0.75), J. Alloys Compd. **858**, 157682 (2021).

[40] C. Kittel and P. McEuen, *Introduction to solid state physics*, global edition ed. (Wiley, Hoboken, NJ, 2018).

[41] J. Ćwik, Y. Koshkid'ko, K. Nenkov, A. Mikhailova, M. Małecka, T. Romanova, N. Kolchugina, and N. A. de Oliveira, Experimental and theoretical analysis of magnetocaloric behavior of $Dy_{1-x}Er_xNi_2$ intermetallics (x=0.25, 0.5, 0.75) and their composites for low-temperature refrigerators performing an ericsson cycle, Phys. Rev. B **103**, 214429 (2021).

[42] J. Ćwik, Y. Koshkid'ko, N. Kolchugina, K. Nenkov, and N. A. de Oliveira, Thermal and magnetic effects in quasi-binary $Tb_{1-x}Dy_xNi_2$ (x = 0.25, 0.5, 0.75) intermetallics, Acta Mater. **173**, 27 (2019).

[43] J. Ćwik, Y. Koshkid'ko, K. Nenkov, E. Tereshina-Chitrova, M. Małecka, B. Weise, and K. Kowalska, Magnetocaloric performance of the three-component $Ho_{1-x}Er_xNi_2$ (x = 0.25, 0.5, 0.75) laves phases as composite refrigerants, Sci. Rep. **12**, 12332 (2022).

[44] T. Gottschall, M. D. Kuz'min, K. P. Skokov, Y. Skourski, M. Fries, O. Gutfleisch, M. G. Zavareh, D. L. Schlagel, Y. Mudryk, V. Pecharsky, and J. Wosnitza, Magnetocaloric effect of gadolinium in high magnetic fields, Phys. Rev. B **99**, 134429 (2019).

[45] M. Balli, S. Jandl, P. Fournier, and A. Kedous-Lebouc, Advanced materials for magnetic cooling: Fundamentals and practical aspects, Appl. Phys. Rev. **4**, 021305 (2017).

[46] J. Lyubina, Magnetocaloric materials for energy efficient cooling, J. Phys. D: Appl. Phys. **50**, 053002 (2017).

[47] O. Gutfleisch, M. A. Willard, E. Brück, C. H. Chen, S. G. Sankar, and J. P. Liu, Magnetic materials and devices for the 21st century: stronger, lighter, and more energy efficient, Adv. Mater. **23**, 821 (2011).

[48] O. Gutfleisch, T. Gottschall, M. Fries, D. Benke, I. Radulov, K. P. Skokov, H. Wende, M. Gruner, M. Acet, P. Entel, and M. Farle, Mastering hysteresis in magnetocaloric materials, Philos. Trans. R. Soc. London A **374**, 20150308 (2016).

[49] K. G. Sandeman, Magnetocaloric materials: The search for new systems, Sci. Mater. **67**, 566 (2012).

[50] G. Porcari, S. Fabbrici, C. Pernechele, F. Albertini, M. Buzzi, A. Paoluzi, J. Kamarad, Z. Arnold, and M. Solzi, Reverse magnetostructural transformation and adiabatic temperature change in Co- and In-substituted Ni-Mn-Ga alloys, Phys. Rev. B **85**, 024414 (2012).

[51] J. Liu, T. Gottschall, K. P. Skokov, J. D. Moore, and O. Gutfleisch, Giant magnetocaloric effect driven by structural transitions, Nat. Mater. **11**, 620 (2012).

[52] C. Li and Z. Wang, Computational modelling and ab initio calculations in MAX phases I, in *Advances in Science and Technology of* $M_{n+1}AX_n$ *Phases* (Woodhead Publishing, Cambridge, UK, 2012), pp. 197–222.